ACS APPLIED MATERIALS & INTERFACES

Research Article

www.acsami.org

Facile Synthesis of Titania Nanowires via a Hot Filament Method and Conductometric Measurement of Their Response to Hydrogen Sulfide Gas

Martin Munz,*[,†] Mark T. Langridge,[‡] Kishore K. Devarepally,[†,‡] David C. Cox,[‡,§] Pravin Patel,[§] Nicholas A. Martin,[†] Gergely Vargha,[†] Vlad Stolojan,[‡] Sam White,[†] and Richard J. Curry*[,‡]

[†]Analytical Science Division, National Physical Laboratory, Teddington, TW11 0LW, United Kingdom

[‡]Advanced Technology Institute, University of Surrey, Guildford, GU2 7XH, United Kingdom

[§]Time Quantum & Electromagnetics Division, National Physical Laboratory, Teddington, TW11 0LW, United Kingdom

Supporting Information

ABSTRACT: Titania nanostructures are of increasing interest for a variety of applications, including photovoltaics, water splitting, and chemical sensing. Because of the photocatalytical properties of TiO_2, chemical processes that occur at its surface can be exploited for highly efficient nanodevices. A facile and fast synthesis route has been explored that is free of catalysts or templates. An environmental scanning electron microscopy (ESEM) system was employed to grow titania nanowires (NWs) in a water vapor atmosphere (~1 mbar) and to monitor the growth in situ. In addition, the growth process was also demonstrated using a simple vacuum chamber. In both processes, a titanium filament was heated via the Joule effect and NWs were found to grow on its surface, as a result of thermal oxidation processes. A variety of nanostructures were observed across the filament, with morphologies changing with the wire temperature from the center to the end points. The longest NWs were obtained for temperatures between ~730 °C and 810 °C. Typically, they have an approximate thickness of ~300 nm and lengths of up to a few micrometers. Cross sections prepared by focused-ion-beam milling revealed the presence of a porous layer beneath the NW clusters. This indicates that the growth of NWs is driven by oxidation-induced stresses in the subsurface region of the Ti filament and by enhanced diffusion along grain boundaries. To demonstrate the potential of titania NWs grown via the hot filament method, single NW devices were fabricated and used for conductometric sensing of hydrogen sulfide (H_2S) gas. The NW electric resistance was found to decrease in the presence of H_2S. Its variation can be explained in terms of the surface depletion model.

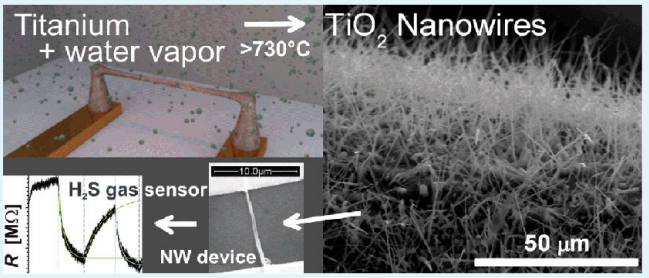

KEYWORDS: *titania (TiO_2) nanowires, semiconductor nanostructures, nanodevices, nanosensors, gas sensing, hydrogen sulfide (H_2S)*

INTRODUCTION

Chemical and biological sensors have profound influence in the areas of detection of environmental toxins, medical diagnosis, and public security. Many of these applications are space-critical and the availability of miniaturized and inexpensive sensors would open up new avenues for the widespread use of such sensors. A new promising approach arises with the recent availability of quasi one-dimensional (1D) nanostructures, nanowires (NWs). Because of their very high surface-to-volume ratio, a major fraction of their atoms are exposed to the molecules of the surrounding medium, and changes in the surface coverage or chemistry are likely to cause significant changes in the physical properties of the nanostructure. To fully realize this potential, each of the many steps involved in creating such a sensor must be brought together in a coherent program that includes NW synthesis, device fabrication, system integration, and an interface to control and monitor device parameters with the ability to sense a critical gas such as hydrogen sulfide (H_2S). It is this challenge that we address in the work reported within this article, based on the use of single TiO_2 NW sensors synthesized using a facile process.

H_2S is a toxic gas that causes olfactory paralysis.[1] Because of this property and the occurrence of H_2S in hydrocarbon reserves and some industrial processes, occupational safety requirements generate a need for highly sensitive, reliable, and low-cost H_2S gas sensors.[1−3] Currently, the workplace exposure limits defined by the Health and Safety Executive (HSE) of the United Kingdom are 10 ppm for a time-weighted average (TWA) over 15 min and 5 ppm for TWA over 8 h.[4] In the United States, it has been proposed to revise the limit down to 1 ppm. In addition, a further need for H_2S sensing at low concentrations may arise from a trend to analyze exhaled breath

Received: March 19, 2012
Accepted: January 17, 2013
Published: January 17, 2013

   dx.doi.org/10.1021/am302655j | ACS Appl. Mater. Interfaces 2013, 5, 1197−1205

for the purpose of diagnostics. In particular, the breath of patients suffering from halitosis is known to contain H_2S in trace amounts.[5] There is therefore an existing and growing need for new higher sensitivity and low-cost H_2S sensors where the use of NWs may provide a solution.

Of the wide range of metal oxide NWs of potential interest, titanium dioxide (TiO_2) is a versatile material that has been investigated extensively, because of its unique optoelectronic and photochemical properties. These include a high refractive index, a high dielectric constant, and excellent optical transmittance in the visible and near-infrared regions, as well as its high performance as a photocatalyst for water splitting[6,7] and for the degradation of organics.[8−10] With a band gap of ∼3.0−3.3 eV, TiO_2 is photocatalytically active only under ultraviolet light (λ < 400 nm) irradiation. Furthermore, titania (Ti_xO_y) NWs, nanorods, or nanobelts have been utilized for chemical sensing applications in a few studies.[11,12] In particular, TiO_2 has been shown to respond to several gases, similar to other metal oxide semiconductors, such as SnO_2 or ZnO. Although less common than sensing of ethanol or carbon monoxide, the detection of H_2S gas using TiO_2 surfaces has been demonstrated. Chaudhari et al.[2] used doped TiO_2 thick films to detect H_2S at concentrations of 200−1000 ppm, with the highest sensitivities observed at operating temperatures within the range of 250−350 °C.

Several synthetic methods for the preparation of nanoscale titania have been reported,[13] including sol−gel reactions,[14] template methods,[15] reactions in reverse micelles,[16] and microwave irradiation.[17] Various morphologies and shapes such as NWs, nanorods, nanotubes, and nanospheres have been observed.[18] Similarly to ZnO structures,[19−21] titania NWs can also be grown via wet chemical techniques.[22] Although such a variety of synthetic methods have been successfully employed, there is a need for simpler methods that allow for integration with microelectronic or microelectromechanical systems (MEMS). In the case of tungsten oxide NWs, several studies have demonstrated a simple approach that requires only a heated tungsten substrate and an oxidizing atmosphere.[23−28] In contrast to the vapor−liquid−solid method,[29] no catalyst particles are needed, the deposition of which increases the complexity of the process and their presence can impair the homogeneity of the resulting nanostructure.

Cox et al.[26] demonstrated the growth of tungsten oxide (W_xO_y) nanostructures by driving an electrical current through a tungsten filament mounted inside the chamber of an environmental scanning electron microscopy (ESEM) system. Depending on the local temperature of the filament, heated by the Joule effect, they found a variety of structures, ranging from thick oxide clusters, to NWs, to platelets. From these findings, it was inferred that the gradient in temperature along the filament affects the NW growth. Similarly, Liu et al.[24] heated a tungsten filament in a vacuum chamber with some air leakage. They grew both undoped and doped tungsten oxide NWs and suggested a vapor−solid growth mechanism. An overview of the published studies where tungsten oxide NWs were grown on top of a tungsten substrate has been provided by Kojima et al.[27] They suggested a solid-phase growth mechanism that involved an amorphous oxide layer on the tungsten surface and migration of tungsten oxide molecules into NW nuclei at irregular points on the tungsten surface.

Relating to the preparation of TiO_2 nanostructures, Liu et al.[30] demonstrated growth of titania NWs under humid conditions in a gas mixture of argon and molecular oxygen (O_2). They employed a quartz tube furnace to heat a titanium substrate to a temperature of ∼850 °C.

In this article, we report on the growth of titania NWs using the hot filament method and their application toward gas sensing. This growth technique is demonstrated both in situ inside the chamber of an ESEM system, and separately in a simple small vacuum chamber into which water vapor is introduced. The use of the ESEM system, although not a necessity, allows for time-resolved imaging of the growing nanostructures. Furthermore, the actual growth process is rapid, typically taking ∼5 min to complete. Following the titania NW growth, employing clean-room techniques and electron beam lithography (EBL), titania NW devices were prepared and tested toward H_2S gas sensing.

EXPERIMENTAL METHODS

(a). Growth of the Titania NWs. Titania nanostructures were synthesized via two methods, using as-received titanium metal wire (Goodfellow, U.K., 99.6% purity, 250 μm diameter). In the first method, the titanium metal filament is clamped between two brass posts (electrically isolated from the substrate holder) and placed on the stage of an ESEM chamber. The mutual distance of the two brass posts was adjusted to ∼1.5 cm, and they were connected to an external low-voltage, high-current, DC power supply. The ESEM chamber (FEI Quanta 200F) was operated in low vacuum mode with a controlled partial atmosphere of water vapor set to a pressure of ∼1 mbar. A potential difference was then applied across the wire until the current reached ∼2 A. The filament emitted IR light, which was observed on the infrared-sensitive camera (chamber-scope) of the instrument, thus clearly indicating the increased temperature of the filament. Following a short period of ∼2−3 min under these conditions, the growth of the nanostructures was observed in real time in the scanning electron microscopy (SEM) system. After removing the substrate holder from the SEM chamber, the titanium filament containing titania nanostructures was suspended in ethanol solution and sonicated to separate nanostructures from the metal filament surface. Subsequently, the titania nanosuspension was used for the fabrication of devices.

In the second method, the titanium filament was again clamped between two brass posts inside a simple vacuum chamber with optical access via a window. The filament was prepared using a procedure that was identical to that used for the ESEM growths and connected by electrical feed-throughs to the current generator. The chamber was then evacuated for ∼7 min prior to bleeding in either dry N_2 (obtained from liquid N_2 boiloff) or wet N_2 (obtained by bubbling dry N_2 through a water column) to obtain a steady base pressure of 5 ± 1 mbar. The current was raised to ∼2 A at a ramping rate of ∼1 A/min to achieve NW growth. Spectroscopy of the filament during heating was performed by placing an optical fiber bundle near the chamber window centered over the filament, with an optical chopper between window and fiber. Light from the fiber dispersed in a spectrometer (Bentham TmC300) prior to detection using a Si or InGaAs detector (Newport 818-SL and 818-IG, respectively) using lock-in amplification (Signal Recovery 7265). Optical filters were used to prevent second-order diffraction of light. The emission spectrum was taken over a heating period of ∼20 min.

A focused-ion beam (FIB) was used to investigate the interface between the grown NWs and the underlying titanium substrate filament. The instrument used was a FEI Nova Nanolab 600 dual-beam FIB. An individual titanium filament was located on a specimen stub and oriented so that the titania NWs were parallel to the ion beam. Using a beam current of 1 nA, a cross section was cut through the center of a NW cluster that extended 2 μm beneath the surface of the filament and was typically 5−8 μm wide.

In addition to the cross sections, thin foil samples were prepared for analysis with the FIB for both 30 kV scanning transmission electron microscopy (STEM) with the electron column in the FIB system and also 200 kV STEM in a Hitachi HD2300A microscope. Raman

spectroscopy was carried using a Renishaw MicroRaman microscope using an excitation wavelength of 514 nm.

For numerical calculation of the temperature profile along the filament the software package Comsol Multiphysics (version 3.3, by Comsol) was employed. A two-dimensional (2D) model was built, putting a 1.3-cm titanium filament between two brass posts measuring 0.5 cm × 2.0 cm. A heating power of 2.0 W was applied in the model. The run time was 120 s to allow for the temperature to equalize. The heat-transfer coefficient value needed was tuned in a way that the hottest temperature was in agreement with the temperature measured using spectroscopy (see Figure S1 in the Supporting Information).

(b). Fabrication of NW Devices. Substrates (*p*-type Si/SiO_2, with an oxide thickness of 250 nm) were cleaned with acetone, isopropanol, and deionized water prior to being coated with a photoresist primer (Rohm and Haas) to improve the adhesion of photoresists. The substrate was then spin-coated with a bilayer photoresist, where a PMGI-SF6 (Microchem) layer was first deposited (spin-coated at 3500 rpm for 10 s) and then baked (at 90 °C for 10 min). This was followed by S1805 (Rohm and Haas) as a top layer (spin-coated at 3500 rpm for 10 s and baked at 85 °C for 5 min). Exposure was carried out in "proximity mode" using an ultraviolet (UV) lamp with an energy density of 40 mJ cm^{-2} (initial reading of the UV lamp was recorded). After the exposure step, the substrate was immersed in MF319 developer solution (Rohm and Haas) for 10 s and then washed with deionized water.

The layout of the mask used is shown in Figure S2(a) in the Supporting Information. It is comprised of 17 sets of quadruple electrodes that were used to connect NWs in two-point or four-point configuration. The electrodes Ti/Au (6 nm/100 nm thickness) were deposited onto the substrate by DC magnetron sputtering (MPS500 by JLS Designs). Since titanium has good adhesion on silicon oxide, a thin titanium layer was deposited first and subsequently gold. The following conditions were observed: argon gas flow, 25 sccm; pressure, 5 mTorr; current, 0.12 A; voltage, 500 V; and set power, 1 kW. The sputtering time was ∼3 min in the case of titanium and ∼12 min in the case of gold. The layer thickness was ∼6 nm and ∼100 nm, respectively.

The terminal contact pads along the edges of the electrode pattern allow for mechanical contact with pins attached to the printed circuit board (PCB) of the NW probe station (see below).

The NWs were then drop-cast from a dilute suspension onto the substrate and allowed to dry. After the deposition of NWs, the connections between their ends and the electrodes were made using EBL. The substrate was examined in the SEM system in the vicinity of the device electrodes and, when a suitable NW was found in the correct location, an image was captured and subsequently used as the basis of the EBL pattern. Typically, ∼30%−50% of the electrode sets on the chip will have a suitable single NW that can be connected. Following imaging, PMMA (A7 by Microchem) was spun onto the substrate and baked on a hot plate for 90 s at 160 °C. The sample is then transferred to the EBL instrument and repositioned to ensure that the devices are at the correct locations. Great care was taken to not expose the device region, except for the required pattern. Following exposure, the solvent methyl isobutyl ketone (MIBK, type Chromosol for HPLC, ≥99.5%) was used to remove the exposed regions and a 5-nm Ti film was sputtered as an adhesion layer, followed by 70 nm of gold. The remaining resist was then lifted off by soaking in acetone, leaving behind the connected NWs. Any NWs not connected at this stage tend to be washed off in this process.

(c). Design of the NW Probe Station. A printed circuit board (PCB) measuring ∼145 mm × 100 mm has been fabricated that contains eight electrical circuits for the readout of NW resistance. One such circuit is shown in Figure S2(c) in the Supporting Information. It represents a constant low-current source, defined by range-setting precision resistors that can be selected by a surface mount switch. It is an extended version of the circuit layout presented in the Supporting Information of ref 31. The current passed through the NW device is connected across the test points. The NW resistance is denoted as R_c. The voltage across the NW ensemble is buffered by an operational amplifier of high input impedance and can be measured by a digital voltmeter or an analog-to-digital converter (ADC). The voltage V_{in} can be applied by a voltage calibrator or a digital-to-analog converter (DAC) and can be varied within a range of ±5 V. Both ADC and DAC are available on a multifunction data acquisition card (type PCIe-7841R, National Instruments) in a personal computer (PC). Via a purpose-made user interface under LabView (version 9.0.1, by National Instruments), the eight circuits of the PCB can be addressed, the drive voltages set or ramped, and the measured output voltages recorded.

The PCB (Figure S2(b) in the Supporting Information) of the NW probe station is designed such that up to eight constant-current sources and voltage buffers can be made available to two carrier chips that can be probed using low-cost gold-plated fingers arranged in a 10 × 10 quad arrangement. In this way, time-consuming wire bonding can be avoided.

A heater block and a thermocouple are integrated into the platform for the carrier chip and driven by a separate analog control module. The temperature of the carrier chip can be varied from room temperature to ∼160 °C.

(d). Gas-Sensing Measurements. A dedicated test chamber exposure facility, fabricated in glass, was used to carry out the gas sensing measurements. A schematic drawing of the facility is given in Figure S3 in the Supporting Information. The design of the facility enabled trace gases to be introduced and be maintained at known concentrations over extended periods of time, under a variety of controlled environmental conditions. The glass facility, which had a volume of ∼27 L, was housed in a compact environmental chamber (Sanyo) that could provide temperature control up to ∼50 °C, and a water vapor generator was also fitted that could deliver and control the required relative humidity up to, nominally, 80% relative humidity (RH) at 20 °C. A fan at the bottom panel of the glass chamber controlled the air speed and assisted in the circulation and mixing of gases if required.

Appropriate bottled gases were delivered to the facility using a mass flow controller (MKS Instruments), which was set to a flow rate of 4.9 L min^{-1} and calibrated using a flow meter (DryCal ML800 series, BIOS International Corporation). For the gas-sensing measurements the exposure facility was employed under "dry" conditions using high-purity nitrogen (metrology grade, BOC) to remove ambient water vapor. Commercial (BOC) and NPL National Standard gas mixtures of H_2S/N_2 were then introduced at a concentration of 80 ppm (±2%) without further dilution.

The PCB with the mounted carrier chip was put on a horizontal platform situated ∼20 cm above the bottom panel of the glass test chamber. To measure the sensing and recovery characteristics of the NW sensors, the gas supply was switched in an alternating manner from N_2 to H_2S/N_2 and back. Typically, a sequence consisted of an initial N_2 exposure (further referenced below as N_2#0) for ∼40 min and 2 or 3 cycles of H_2S/N_2 and subsequent N_2 exposures (below referred to as H_2S#*i* and N_2#*i*, with *i* = 1, 2, or 3, respectively). The exposure times were in the range of 45−60 min. The NW device was operated in the linear regime of its *I*−*V* curve. The set constant current supplied to the device was −175 nA, corresponding to an input voltage (V_{in}) of approximately −1.75 V.

RESULTS AND DISCUSSION

Characterization of the Growth Process and the Resulting Titania Nanostructures. Through the Joule heating process described above, titania NWs were synthesized with a thickness in the range 100−500 nm and a length up to several micrometers (Figure 1). The NWs grew on top of the hot metal filament and tend to show a tapered shape with the thicker end of ∼300−500 nm near the filament. Typically, they taper off toward the outer end, where they measure ∼100 nm or less. Further variations in the measured thickness also result from the beltlike shape of the NWs.

The size and shape of the titania nanostructures are dependent on their position along the titanium filament,

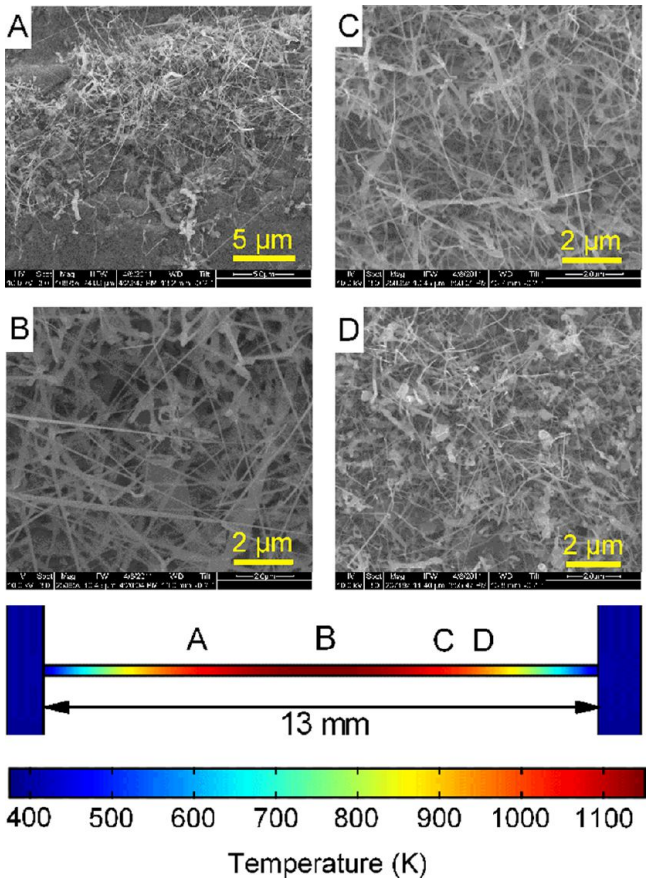

Figure 1. SEM micrographs of titania nanostructures grown on top of a Ti filament. The length of the scale bar is 5.0 μm in panel (a) and 2.0 μm in panels (b)−(d). The micrographs were taken at different positions on the filament long axis, as indicated in the schematic at the bottom of the figure. It shows the filament clamped between two brass posts and the related temperature distribution. The hottest region is in the middle of the filament.

since the local temperature is a function of the distance from the electrodes. As the filament was ohmically heated and connected to relatively large heat-sinking posts, a temperature gradient was established along the filament with the central region being the hottest and regions near the posts being the coolest. By 2D thermal modeling with input from optical spectroscopy to measure the thermal radiation emitted (see Figure S1 in the Supporting Information), the temperature of the central region of the filament was estimated to be ∼1150 K (Figure 1).

The obtained nanostructures are comprised of NWs and nanobelts that change in morphology from the hottest region of the filament to the coolest region, where only a rough oxide film was observed. The NWs useful for this study are observed to grow over most of the central half of the filament (Figures 1b and 1c). The SEM images given in Figures 1a and 1d, taken at some distance from the filament end, show a low density of short NWs or nanorods that grow on top of a rough filament surface.

Notably, the growth process only takes a few minutes. The entire process, including mounting and connecting the sample, evacuating the chamber, and heating the filament, requires a total of ∼20 min.

It should be mentioned that the in situ configuration allows for SEM imaging while the NWs are growing. Typically, the electron beam is left on and the central region of the filament imaged to observe growth in real time. However, the electron beam is found to have no effect on the growth process as determined via control experiments with the electron beam turned off for the duration of the growth. Furthermore, growth of NWs using the second method in a simple vacuum chamber, as described above, produced similar growth when wet N_2 was used. In the case of using dry N_2 in this latter growth method, no NWs or formation of an oxide layer on the titanium filament was observed following heating. These observations show that the NW growth originates from the interactions of water vapor with the heated titanium filament.

High-resolution transmission electron microscopy (HRTEM) images of NWs grown by the hot filament method show that they are single crystalline (Figure 2a). The (110)

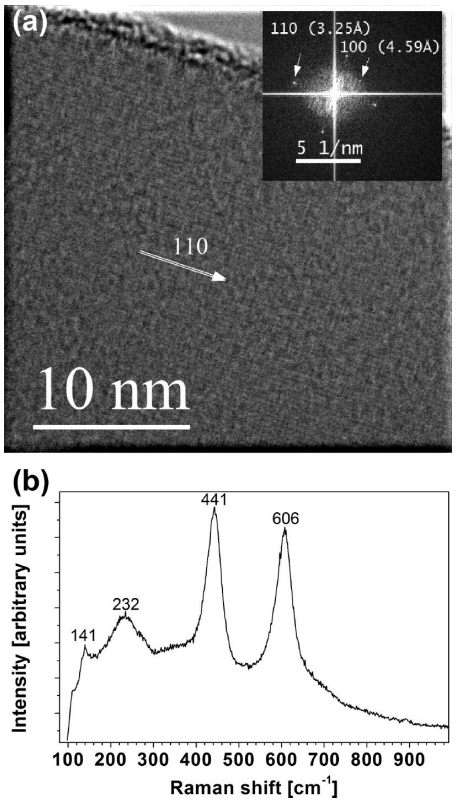

Figure 2. (a) HRTEM image of a single NW (inset shows a fast Fourier transform (FFT) of the image). The TEM image shows (110) lattice planes perpendicular to the long axis of the NW. Their interplanar distance is 3.25 ± 0.05 Å; also visible are the (100) lattice plane fringes, at 4.59 ± 0.08 Å, suggesting a rutile structure. To increase the visibility of the fringes, a bandpass filter has been applied. (b) Raman spectrum of titania nanowires with peaks at 141, 236, 440, and 605 cm^{-1}, also suggesting a rutile structure.

lattice planes are clearly observed with their interplanar distance measured to be ∼3.25 Å, accompanied by the presence of (100) lattice plane fringes measured to be 4.59 ± 0.08 Å apart (inset Figure 2a), thus it can be concluded that the TiO_2 crystal structure is rutile (in contrast, the interplanar distance of TiO_2 anatase is ∼3.51 Å). Electron energy loss spectroscopy (EELS) data (not shown) confirmed that the NWs consist of TiO_2. To further confirm the rutile nature of the TiO_2 NWs, Raman spectroscopy was performed on as-grown samples (Figure 2b). Raman peaks consistent with a rutile structure are observed at

dx.doi.org/10.1021/am302655j | ACS Appl. Mater. Interfaces 2013, 5, 1197−1205

141, 236, 440, and 605 cm^{-1} in agreement with other reports.[32−34]

To quantify the variation in the NW dimensions with their position on the filament long axis, NWs were imaged and their dimensions measured at six different locations. In this case, the growth conditions were 0.9 mbar and 2.0 A. Areas around five equidistant points outward from the filament center to the region where no NWs occurred were analyzed, plus one area on the opposite side of the filament center (−3 mm). At each location, ∼100 NWs were analyzed (ranging from 66 to 139, as shown in Table 1). The resulting average NW lengths and

Table 1. Variation in Average Nanowire (NW) Length, Relative to Distance from the Filament Center

distance from filament center [mm]	average NW length [μm]	standard deviation of NW length [μm]	number of NWs analyzed	calculated temperature [°C]
−3.0	3.4	1.7	111	734
0.0	0.88	0.49	124	877
1.0	7.9	5.1	66	860
2.0	10.5	3.8	106	814
2.5	4.0	3.3	90	780
3.0	2.8	2.6	139	734
3.5	1.68	0.59	93	676

related standard deviations are also listed in Table 1. Histograms of the NW lengths measured at each location are provided in Figure S4 in the Supporting Information, in which Gaussian fits are also included, from which the data in Table 1 resulted.

As can be seen from Table 1, the shortest NWs were found in the center of the filament and the longest NWs occurred at a distance of ∼1−2 mm from this point, suggesting that, at the given pressure, this region represented the preferable temperature range for NW growth. Furthermore, the standard deviation values indicate that, ∼2 mm from the center, the NWs were the most uniform in length, since the ratio of standard deviation and average length is lowest at these points. Considering that the average NW lengths at −3 and +3 mm from the center are similar (Table 1), it can be concluded that the growth conditions at both positions were identical and that the temperature profile along the filament was symmetrical.

Assuming a heating power of 2.0 W and a run time of 120 s to allow for stationary conditions, numerical calculation of the temperature profile across the filament delivered a maximum temperature of ∼877 °C (1150 K). From spectroscopic measurements (Figure S1 in the Supporting Information), it was estimated that the heat-transfer coefficient for convective heat loss is ∼310.5 W m^{-2} K^{-1}.

A large part of the calculated temperature profile was above ∼727 °C (1000 K), with the end parts of the filament decreasing in temperature due to the heat sink effect of the two brass posts (Figure 1). The calculated temperatures at the locations where NWs were imaged and analyzed are provided in Table 1. A plot of the average NW length versus the calculated local temperature is shown in Figure 3. Bearing in mind the error margin, it can be inferred that the longest NWs grow at temperatures in the range between ∼734 °C (1007 K) and ∼814 °C (1087 K). In this range, the average NW length is ≥4 μm. However, for higher temperatures, up to ∼860 °C (1133 K), long NWs also were found, with a wider length distribution. Since the model is symmetrical about the filament

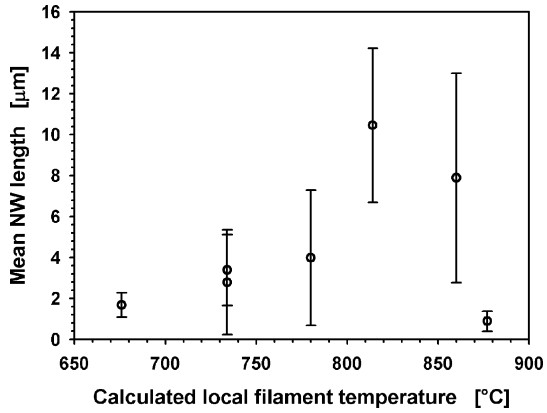

Figure 3. Plot of the average NW length versus the calculated filament temperature.

center, it suggests that the locations at +3.0 and −3.0 mm have the same temperatures, in agreement with the similar values of the average NW length measured.

A likely reason for the occurrence of comparatively short NWs in the central and hottest region is a high rate of oxidation, which may interfere with the growth process.

Variation of the chamber pressure for a given electric current affects the temperature gradient along the filament. Growth was undertaken at 0.1, 0.3, 0.6, and 0.9 mbar, with an electric current of 2.0 A and a growth time of up to 12 min. Visual inspection of the filament following each experiment in the SEM system revealed that no NWs had grown at a pressure of 0.1 mbar; instead, a uniform film was observed. The greatest yield was found for pressures in the range of 0.6−0.9 mbar. The clusters with the highest density of NWs from a single nucleation point were found for chamber pressures of 0.6 and 0.8 mbar. Also, the largest overall coverage of the filament with NWs was observed for 0.6 mbar.

It should be noted that the yield was also dependent on the magnitude of the electrical current. A lower surface coverage with NWs was observed for currents of 1.5 and 2.5 A. Hence, a chamber pressure of 0.6 mbar and a filament current of 2.0 A were noted as the preferred growth condition.

To develop a better understanding of the growth mechanism, sections were milled into the base of NW clusters. The milling was achieved using the gallium ion beam available with the SEM−FIB system. The NWs under investigation were grown at 0.6 mbar and 2.0 A. By milling inward, toward the root of the clusters, the subsurface morphology was revealed. SEM micrographs of two resulting cross sections are given in Figure 4. In the case of the section shown in Figure 4b, a thin layer of platinum was deposited on the cluster surface to hold the NWs in place.

As shown in Figure 4, the substrate beneath the NW cluster is porous. In particular, a dark band can be seen running beneath the root of the clusters. The band seems to represent a region where nanoscale pores occur.

With the aim of creating a thin foil suitable for TEM analysis, another cluster was ion-milled. In Figure 5, dark-field and bright-field images are shown that were taken with a STEM detector. These images show distinct lines that can be attributed to grain boundaries (GBs). Adjacent grains in the metal having different crystal faces lead to a change in the interaction with electrons transmitted through the sample. Hence, the distinct borderlines can be assigned to GBs.

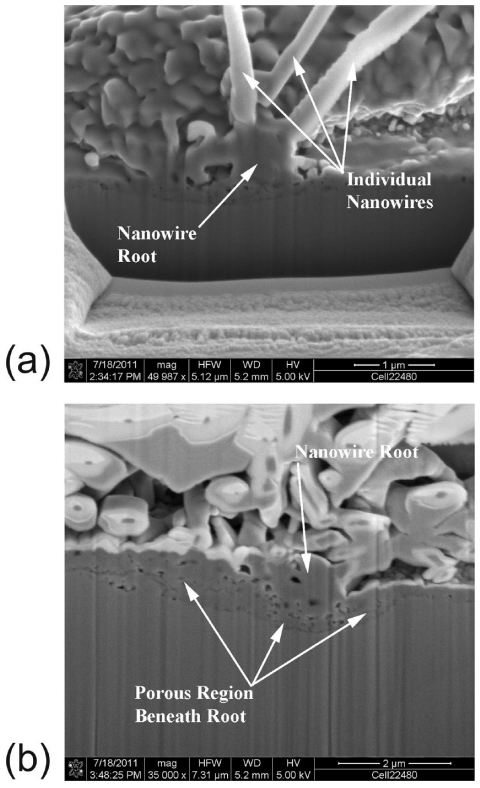

Figure 4. SEM micrographs of cross-sectional surfaces of two different NW clusters. The cross sections were prepared by ion-beam milling. The lengths of the scale bars in panel (a) and (b) are 1 and 2 μm, respectively.

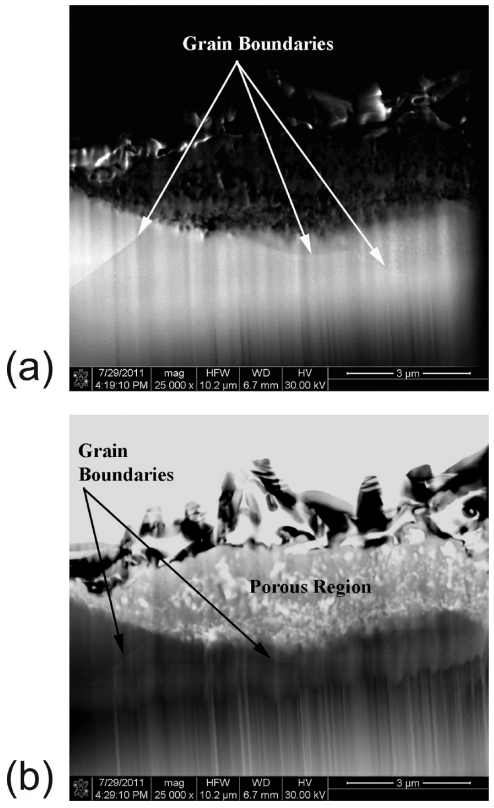

Figure 5. (a) Dark-field and (b) bright-field images of a thin section milled out from beneath a NW cluster. Hard contrasts can be seen that represent possible GBs. The length of the scale bars is 3 μm.

The presence of GBs beneath NW clusters is a key indicator as to why NWs grow at specific locations on the filament surface. Diffusion rates are known to be increased along GBs.[35,36] Therefore, titanium will be able to diffuse faster toward the filament surface as the oxidation is proceeding and the GBs are widening. In this way, material can be delivered quickly to a growth region for NWs to form.

Suggested Growth Mechanism. The ion-milling experiments have shown that the presence of several GBs results in a porous region forming underneath the NWs. Because of an increased diffusion along GBs, oxygen (either thermally released from H_2O upon contact with the hot filament[37] or via catalysis upon interaction with any excited TiO_2 present[6]) will diffuse preferentially along GBs located near the filament surface. Oxygen will penetrate more quickly at these points and oxidize the filament, thus resulting in the porous structure observed underneath the NWs.

As the growth continues, an outer titania shell forms on the filament surface and around the subsurface GBs (Figure 6a). As the titania shell thickens, the stresses around the Ti/titania interfacial region increase and eventually the layer cracks, thus providing further pathways into the material (Figure 6b). Indeed, the experiments have shown a delay of ~2−3 min between the start and the sudden appearance of NWs. This delay can be considered an incubation time (see Figure S5 in the Supporting Information).

After the formation of these pathways, oxygen is more readily available to the titanium being brought up the GB; that is, the supply of oxygen is not limited by slow bulk diffusion through the titania shell. In this way, a good supply with both titanium and oxygen is achieved, allowing for fast growth of NWs. Figure

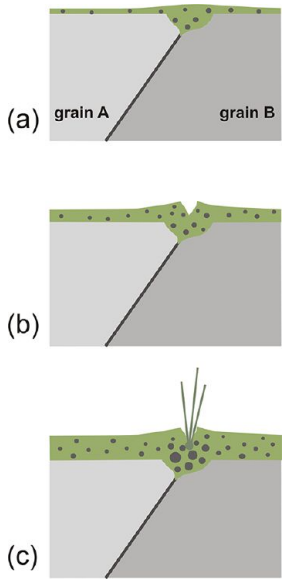

Figure 6. Schematic representation of the NW growth process. (a) A porous titania layer (green) is growing on top of the heated Ti filament (gray), which is polycrystalline. Oxygen species are supplied from the gaseous phase and Ti species are supplied via the Ti surface and the GB (black line). (b) With increasing thickness of the titania layer, interfacial stresses develop and stress relaxation occurs via cracks and formation of voids. (c) NWs are growing at the titania surface, pushed upward by mechanical stresses. The pores beneath the root of the NWs are enlarged.

6c illustrates the growth of NWs above a GB. Similarly, NW growth can also occur near the middle of a grain if its surface allows for fast diffusion of titanium supplied via adjacent GBs.

Interestingly, a similar mechanism has been proposed for the growth of metal whiskers.[38,39] A reaction between oxygen and titanium leads to volume expansion, thus resulting in compressive stresses that can push the whiskers upward.

With ongoing growth, material diffuses upward from the nucleation point toward the tip of the NW. It is likely that this is due to a fast surface diffusion and that the diffusion rate scales with the local temperature. Above a certain temperature the diffusion along the NW long axis may become less favorable, thus resulting in shorter but thicker NWs. The longest NWs were found for temperatures in the range of 760−830 °C, in reasonable agreement with the study by Liu et al.,[30] where the synthesis was undertaken at 850 °C. However, note that their growth experiments were conducted under standard pressure, rather than under vacuum conditions.

NWs can form if titania builds up faster on one crystal face. When a change in the crystal structure occurs, such as a stacking fault, the dominating diffusion direction will be altered and result in a different growth direction. Indeed, the grown NWs show kinks that can be associated with stacking faults.

Further support for the hypothesis of NW growth by preferential diffusion along GBs arises from the observation that the NWs tended to grow in lines along the long axis of the wire. Since the titanium filament had been produced in a cold drawing process, its grains—and, therefore, the majority of grain boundaries—will be elongated in the direction of the long axis. Since NWs were typically found to nucleate in lines parallel to the filament long axis, it can assumed that long GBs run underneath the NW clusters, which act as nucleation points.

Finally, it should be noted that the presence of water vapor is crucial for the NW growth. Water vapor is known to enhance the formation of oxygen vacancies.[30,40] This, in turn, increases the diffusivity of oxygen ions and reduces the diffusivity of Ti interstitials.[30]

Gas-Sensing Measurements. Devices with a single titania NW were fabricated and evaluated as sensors in the presence of H_2S gas at low concentrations in the ppm range. Schematics of the NW probe station and of the gas-sensing facility are given in Figures S2 and S3, respectively, in the Supporting Information. As can be seen from the SEM image (Figure 7a) of the device, the titania NW is slightly tapered, with an average width of ∼420 nm. The channel length is ∼10.6 μm. The plot in Figure 7b shows the response of a single NW device to 80 ppm of H_2S gas in N_2.

The temperature of the platform where the carrier chip is mounted was ∼140 °C. Initialization was achieved by exposure to N_2 gas (segment N_2#0). Then diluted H_2S gas was introduced into the chamber for ∼50 min, followed by a period of N_2 gas flow at the same flow rate to remove the H_2S. This cycle of alternating exposure to H_2S/N_2 and N_2 gas was repeated three times. Accordingly, the plot shows three response segments where the resistance drops and three subsequent recovery segments where the resistance increases again.

Upon exposure to H_2S gas, the NW resistance (R_c) decreases (Figure 7b). The relative change in R_c over the first H_2S exposure (H_2S#1) is ∼11% of its value at the beginning of the segment H_2S#1. Subsequent increase of the resistance upon exposure to pure N_2 (Figure 7b) shows that the NW device

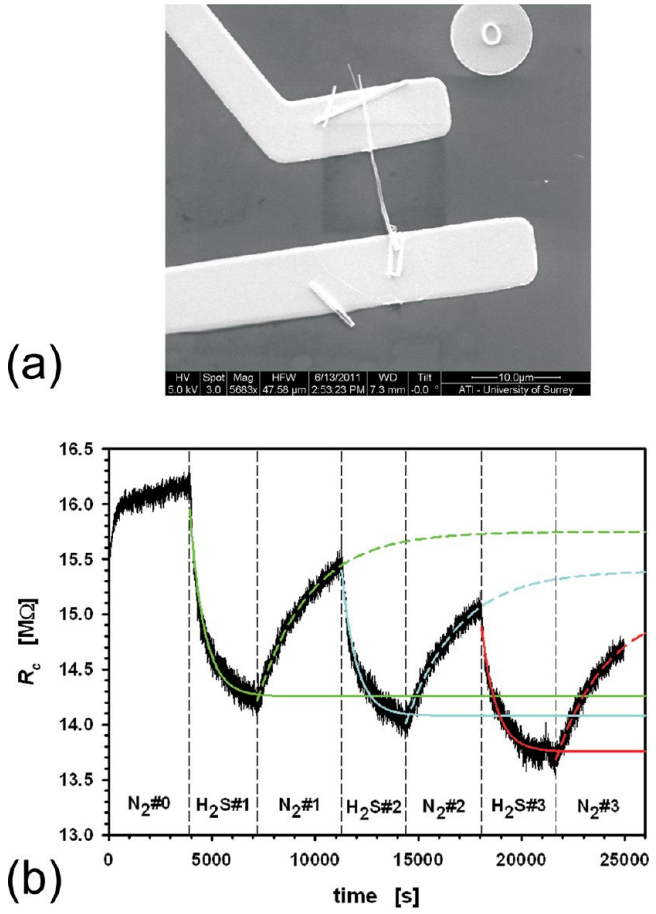

Figure 7. (a) SEM image of a device with a single titania NW. The length of the scale bar is 10.0 μm. (b) Response of the NW device to 80 ppm of H_2S gas in N_2. The colored lines (green denotes cycle 1, blue denotes cycle 2, and red denotes cycle 3) show the fit results using single exponential functions. The solid and the dashed lines are related to response and recovery segments, respectively.

recovers and is ready for further sensing events. The single exponential fit of the decay in R_c over the first H_2S exposure (H_2S#1) gives an apparent response time of ∼705 s. For the given gas flow rate (∼4.9 L/min) and volume of the environmental chamber (∼27 L), however, the time required to expel the gas initially contained in the chamber, which, in this case, was N_2, is of the same order. Thus, the observed response time is limited by the gas exchange rate and represents the response of the entire system, consisting of both the chamber and the NW device, rather than just that of the NW device specifically. We note, however, that the purpose of the experiment was to demonstrate the H_2S gas-sensing capability of TiO_2 NWs as grown by the hot filament method. A detailed kinetic analysis, which is beyond the scope of this work, would require the development of a different gas injection system/procedure, with gas exchange times well below the response and recovery times of the sensor.

Oxygen initially adsorbed on the titania surface captures electrons, thus leaving behind positively charged donor ions and generating an electric field between the donor ions and negatively charged oxygen ions, such as O_2^- or O^-.[2] The resulting surface potential causes a depletion region, thus reducing the cross section of the conduction channel and increasing the electrical resistance of the titania NW. Conversely, in the presence of a reducing gas (electron

donor), such as H_2S, the amount of oxygen ions adsorbed decreases, thus reducing the surface potential and the associated depletion of free electrons. As a result, a decrease in the NW resistance is observed. That is, the observed sensor response can be interpreted in terms of the surface depletion model.[41−43]

To test the selectivity of the device, the chamber was purged with 508 ppm of CO gas in synthetic air. Since CO is chemically reducing (similar to H_2S), any response would indicate a potential for cross-sensitivity with other gases. In such measurements, no significant change in device signal was detected.

If a linear device response-to-concentration relationship is assumed for the regime between 0 and 80 ppm H_2S, the limit of detection (LOD) of the sensor can be estimated from its response to 80 ppm H_2S and the signal noise level. In the linear part of segment N_2#0 of Figure 7b, the noise level, σ, is measured to be ∼0.042 MΩ (see Figure S6 in the Supporting Information). The total resistance change over the first exposure to 80 ppm H_2S (Figure 7b, H_2S#1) is $\Delta R_c \approx 1.53$ MΩ. Approximating the lowest detectable resistance change with 4σ, the LOD is given by $(4\sigma/\Delta R_c) \times 80$ ppm ≅ 8.8 ppm. This result is consistent with experimental tests at 10 ppm H_2S, which showed signal variations close to the noise level.

These experiments demonstrate the response of titania NWs to H_2S gas of 80 ppm concentration. The sensitivity can be limited by the reactivity of the reducing gas or the number of active sites for oxygen adsorption on the NW surface. Chemical functionalization strategies can be employed to condition the NW surface and enhance the sensor characteristics.

For instance, Hu et al.[12] demonstrated various approaches to increase the sensitivity and selectivity toward ethanol by chemical modification of a TiO_2 nanobelt surface. Also, sensitization via titania doping has been demonstrated. In particular, doping of TiO_2 films with Pd was found to result in an increased sensitivity toward H_2S, whereas the response to CO, H_2, and liquid petroleum gas (LPG) was almost unchanged.[2] This indicates a strong potential of titania for selective detection of H_2S. The sensor response to H_2S is likely to be assisted by the fact that the molecule is prone to dissociation, because of the low H−SH bond energy.[29,44]

If required, the selectivity can be increased by an electronic nose approach where several NW devices with different NW materials or NW surface chemistries are combined and pattern recognition or similar analysis techniques are employed to enhance the sensor performance.[41,45]

Furthermore, the sensor characteristics are also dependent on the operation conditions. An increase in temperature is likely to increase the rates of surface reaction and desorption. In their study of the gas-sensing properties of nanosized TiO_2 thick films, Chaudhari et al.[2] observed significantly increased sensitivities for operating temperatures in the range of 250−350 °C. Hence, improved sensing characteristics can be expected for operation temperatures above 140 °C. Moreover, when exposed to UV light, TiO_2 shows photocatalytic effects[8] that can be exploited to increase both the sensitivity and selectivity of the sensor.

CONCLUSIONS

Water-assisted growth of titania nanowires (NWs) has been realized by generating a low water vapor pressure inside the chamber of an environmental scanning electron microscopy (ESEM) system or a simple vacuum chamber. Joule heating of a titanium filament led to a temperature profile across the filament, and high-aspect-ratio NWs grew in regions with a temperature of ∼730−810 °C. Typically, the titania NWs observed in these regions have an approximate thickness of ∼300 nm and a length up to a few micrometers. The preferred growth conditions were a water vapor of ∼1 mbar and a current of ∼2.0 A through a titanium filament ∼250 μm in diameter.

As the growth can be observed in situ, this approach allows for scanning electron microscopy (SEM) imaging to be performed readily. Furthermore, it is a fast and facile method that requires neither a catalyst nor a template. Because of its simplicity and comparatively short growth times (on the order of minutes), this thermal oxidation approach could allow for development toward a roll-to-roll process with a high throughput.[46] It has potential for integration with manufacturing techniques that are established in the semiconductor industry and could also be developed toward the growth of metal oxide NWs on top of metal films deposited on microelectromechanical system (MEMS) components.

Analysis of the subsurface region beneath clusters of NWs revealed porous layers. From the experimental findings, it can be inferred that oxidation of the titanium filament surface results in mechanical stresses that drive the upward diffusion of titania for the growth of NWs. Fast diffusion occurs preferentially along grain boundaries (GBs). Scanning transmission electron microscopy (STEM) imaging confirmed the presence of GBs in the subsurface region of the titanium filament.

To demonstrate the potential of titania NWs grown via the hot filament method, single NW devices were fabricated and tested for the purpose of H_2S gas sensing at low concentrations. In particular, they showed a clear conductometric response to 80 ppm H_2S gas and a limit of detection of ∼10 ppm. The NW electric resistance was found to decrease in the presence of H_2S. Modulation of the depletion layer thickness by reactions between the titania NW surface and the H_2S gas molecules leads to variations in the NW electrical conductivity. Future work may develop strategies for optimization of the device performance.

ASSOCIATED CONTENT

Supporting Information

Thermoluminescence analysis, a hierarchical representation of the main components of the NW probe station, a schematic of the gas-sensing facility, histograms of NW lengths at various locations on the filament, SEM images at various elapsed times during the NW growth, and an evaluation of the NW device noise level. This material is available free of charge via the Internet at http://pubs.acs.org.

AUTHOR INFORMATION

Corresponding Author

*E-mail addresses: martin.munz@npl.co.uk (M.M.), r.j.curry@surrey.ac.uk (R.J.C.).

Notes

The authors declare no competing financial interest.

ACKNOWLEDGMENTS

This work is funded by the National Measurement System of the UK Department for Business, Innovation and Skills through the Strategic Research Programme. We thank Steve Smith

(NPL) for technical assistance with the gas sensing test chamber.

REFERENCES

(1) Khanna, A.; Kumar, R.; Bhatti, S. S. *Appl. Phys. Lett.* **2003**, *82*, 4388−4390.
(2) Chaudhari, G. N.; Bende, A. M.; Bodade, A. B.; Patil, S. S.; Manorama, S. V. *Talanta* **2006**, *69*, 187−191.
(3) Chen, J.; Wang, K.; Hartman, L.; Zhou, W. *J. Phys. Chem. C* **2008**, *112*, 16017−16021.
(4) *HSE OCE6 document of the UK Health and Safety Executive (HSE)*. Available via the Internet at http://www.hse.gov.uk/pubns/guidance/oce6.pdf.
(5) Washio, J.; Sato, T.; Koseki, T.; Takahashi, N. *J. Med. Microbiol.* **2005**, *54*, 889−95.
(6) Cowan, A. J.; Tang, J. W.; Leng, W. H.; Durrant, J. R.; Klug, D. R. *J. Phys. Chem. C* **2010**, *114*, 4208−4214.
(7) Wang, G.; Wang, H.; Ling, Y.; Tang, Y.; Yang, X.; Fitzmorris, R. C.; Wang, C.; Zhang, J. Z.; Li, Y. *Nano Lett.* **2011**, *11*, 3026−3033.
(8) Hashimoto, K.; Irie, H.; Fujishima, A. *Jpn. J. Appl. Phys., Part 1* **2005**, *44*, 8269−8285.
(9) Nag, M.; Basak, P.; Manorama, S. V. *Mater. Res. Bull.* **2007**, *42*, 1691−1704.
(10) Hartmann, P.; Lee, D. K.; Smarsly, B. M.; Janek, J. *ACS Nano* **2010**, *4*, 3147−3154.
(11) Rout, C. S.; Kulkarni, G. U.; Rao, C. N. R. *J. Phys. D: Appl. Phys.* **2007**, *40*, 2777−2782.
(12) Hu, P.; Du, G.; Zhou, W.; Cui, J.; Lin, J.; Liu, H.; Liu, D.; Wang, J.; Chen, S. *ACS Appl. Mater. Interfaces* **2010**, *2*, 3263−3269.
(13) Chen, X.; Mao, S. S. *Chem. Rev.* **2007**, *107*, 2891−2959.
(14) Wang, C. C.; Ying, J. Y. *Chem. Mater.* **1999**, *11*, 3113−3120.
(15) Lee, J.; Choi, J.; Lee, J.; Choi, S. K.; Chun, H. D. *Nanotechnology* **2005**, *16*, 1449−1453.
(16) Lim, K. T.; Hwang, H. S.; Ryoo, W.; Johnston, K. P. *Langmuir* **2004**, *20*, 2466−2471.
(17) Jena, A.; Vinu, R.; Shivashankar, S. A.; Madras, G. *Ind. Eng. Chem. Res.* **2010**, *49*, 9636−9643.
(18) Jong-Heun, L. *Sens. Actuators, B* **2009**, *140*, 319−336.
(19) Liu, B.; Zeng, H. C. *J. Am. Chem. Soc.* **2003**, *125*, 4430−4431.
(20) Wahab, R.; Kim, Y. S.; Lee, K.; Shin, H. S. *J. Mater. Sci.* **2010**, *45*, 2967−2973.
(21) Devarepally, K. K.; Cox, D. C.; Fry, A. T.; Stolojan, V.; Curry, R. J.; Munz, M. *J. Mater. Sci.* **2012**, *47*, 1893−1901.
(22) Shyue, J. J.; Cochran, R. E.; Padture, N. P. *J. Mater. Res.* **2006**, *21*, 2894−2903.
(23) Gu, G.; Zheng, B.; Han, W. Q.; Roth, S.; Liu, J. *Nano Lett.* **2002**, *2*, 849−851.
(24) Liu, K.; Foord, D. T.; Scipioni, L. *Nanotechnology* **2005**, *16*, 10−14.
(25) Hong, K. Q.; Xie, M. H.; Wu, H. S. *Nanotechnology* **2006**, *17*, 4830−4833.
(26) Cox, D. C. S., V.; Chen, G.; Silva, S. R In situ observation of the growth of tungsten oxide nanostructures. In *Microscopy of Semiconducting Materials*, Cullis, A. G., Midgley, P. A., Eds.; Springer Proceedings in Physics, Vol. *120*; Springer: Dordrecht, The Netherlands, 2007; pp 277−280.
(27) Kojima, Y.; Kasuya, K.; Nagato, K.; Hamaguchi, T.; Nakao, M. *J. Vac. Sci. Technol., B* **2008**, *26*, 1942−1947.
(28) Kasuya, K.; Ooi, T.; Kojima, Y.; Nakao, M. *Appl. Phys. Express* **2008**, *1*, 034005.
(29) Lu, J. G.; Chang, P.; Fan, Z. *Mater. Sci. Eng., R.* **2006**, *52*, 49−91.
(30) Liu, H.; Zhang, Y.; Li, R.; Cai, M.; Sun, X. *J. Nanopart. Res.* **2011**, *13*, 385−391.
(31) Hernandez-Ramirez, F.; Prades, J. D.; Tarancon, A.; Barth, S.; Casals, O.; Jimenez-Diaz, R.; Pellicer, E.; Rodriguez, J.; Juli, M. A.; Romano-Rodriguez, A.; et al. *Nanotechnology* **2007**, *18*, 495501.
(32) Melendres, C. A.; Narayanasamy, A.; Maroni, V. A.; Siegel, R. W. *J. Mater. Res.* **1989**, *4*, 1246−1250.
(33) Porto, S. P. S.; Fleury, P. A.; Damen, T. C. *Phys. Rev.* **1967**, *154*, 522−526.
(34) Yeh, C. N.; Chen, Y. M.; Chen, C. A.; Huang, Y. S.; Tsai, D. S.; Tiong, K. K. *Thin Solid Films* **2010**, *518*, 4121−4125.
(35) Schmalzried, H. Solid State Reactions. In *Solid State Reactions*; Academic Press: New York, 1974.
(36) Herzig, C. D.; Divinski, S. V. *Mater. Trans.* **2003**, *44*, 14−27.
(37) O'Brien, J. E. In *ASME 2008 International Mechanical Engineering Congress and Exposition (IMECE2008)*, Boston, MA, USA, 2008; pp 639−651.
(38) Barsoum, M. W.; Hoffman, E. N.; Doherty, R. D.; Gupta, S.; Zavaliangos, A. *Phys. Rev. Lett.* **2004**, *93*, 206104.
(39) Galyon, G. T.; Palmer, L. *IEEE Trans. Electron. Packag. Manuf.* **2005**, *28*, 17−30.
(40) Shannon, R. D. *J. Appl. Phys.* **1964**, *35*, 3414−3416.
(41) Sysoev, V. V.; Button, B. K.; Wepsiec, K.; Dmitriev, S.; Kolmakov, A. *Nano Lett.* **2006**, *6*, 1584−1588.
(42) Lupan, O.; Ursaki, V. V.; Chai, G.; Chow, L.; Emelchenko, G. A.; Tiginyanu, I. M.; Gruzintsev, A. N.; Redkin, A. N. *Sens. Actuators, B* **2010**, *144*, 56−66.
(43) Fan, Z. Y.; Wang, D. W.; Chang, P. C.; Tseng, W. Y.; Lu, J. G. *Appl. Phys. Lett.* **2004**, *85*, 5923−5925.
(44) Wang, C.; Chu, X.; Wu, M. *Sens. Actuators, B* **2006**, *113*, 320−323.
(45) Star, A.; Joshi, V.; Skarupo, S.; Thomas, D.; Gabriel, J. C. P. *J. Phys. Chem. B* **2006**, *110*, 21014−21020.
(46) Sunkara, M. K.; Pendyala, C.; Cummins, D.; Meduri, P.; Jasinski, J.; Kumar, V.; Russell, H. B.; Clark, E. L.; Kim, J. H. *J. Phys. D: Appl. Phys.* **2011**, *44*, 174032.